Journal of Computational Science 72 (2023) 102083

Contents lists available at ScienceDirect

Journal of Computational Science

journal homepage: www.elsevier.com/locate/jocs

Efficient dynamic modeling of soft tissue deformation using a WSC-integrated order reduction method

Wenguo Hou [a], Jing Xiong [b], Zeyang Xia [a,c,*]

[a] Soft Robotics Research Center, Shenzhen Institute of Advanced Technology, Chinese Academy of Sciences, Shenzhen, 518055, Guangdong, China
[b] Research Center for Medical Robotics and Minimally Invasive Surgical Devices, Shenzhen Institute of Advanced Technology, Chinese Academy of Sciences, Shenzhen, 518055, Guangdong, China
[c] CAS Key Laboratory of Human–Machine Intelligence-Synergy Systems, Shenzhen Institute of Advanced Technology, Chinese Academy of Sciences, Shenzhen, 518055, Guangdong, China

ARTICLE INFO

Keywords:
Soft tissue deformation
Computational model
Order reduction method

ABSTRACT

Background and Objectives: Computational modeling of soft tissue deformation is a fundamental issue for engineering assistive medical procedures. However, existing methods are not suitable for online clinical scenes as these methods are not efficient due to high computational cost and complexity.
Methods: A new Weighted Skinning and Cubature Integrated (WSC-integrated) order reduction method is proposed for dynamic modeling of soft tissue deformation. The presented method includes two integrated-based schemes for construction of sub-space and estimation of internal elastic forces: a weighted skinning integrated scheme and a cubature integrated scheme. The weighted skinning integrated scheme derived from handle-based reduced order method is adopted to construct a reduced-order sub-space, in which dynamics of soft tissue are governed by low-order system equations. The cubature integrated scheme is adopted to estimate internal elastic forces of soft tissue. The proposed method relies on integration schemes both in sub-space construction and internal forces estimation instead of precomputation of soft tissue deformation snapshots, making it possible to achieve efficient computation of soft tissue deformation.
Results: Compared to a finite element method in full-space for computing soft tissue deformation, the proposed method has a relative root mean square error for strain–stress and volumetric responses is 4.27 % and 3.11 %, respectively, and for rotation-moment and volumetric responses is 2.15 % and 2.63 %, respectively. The computation time of the proposed method achieve significant improvement (ranges from 37× to 54×) with proper choice of sample handles and elements. Simulation of left ventricle dynamics based on the proposed method takes (21.81 ms) approximately 1/43 amount of computation time of the finite element method during online stage, and difference between their results is negligible (with relative root mean square error of 2.4 %).
Conclusions: The simulation results and comparison validated that the proposed method presents higher computational efficiency and comparable accuracy to the finite element method in full-space. The high degree of computational efficiency and accuracy of the proposed method makes it suitable for online clinical scenes.

1. Introduction

Computational modeling of soft tissue deformation has been proven to be an effective way for developments of clinical applications, such as disease diagnosis [1,2], virtual surgery simulation [3,4] and surgical navigation [5]. A high-resolution model with precise anatomical details is expected to reveal physiological information and to predict treatment outcomes [6,7]. Simulation of soft tissue deformation with finite element method (FEM) can achieve accurate results with multi physiology and physics aspects but require a large amount of computational cost. The order reduction method has been incorporated in order to reduce the computational cost, where an inexpensive low-dimensional system that approximates the original system is constructed in offline stage and evaluated fast in online stage [8,9]. However, the existing order

* Corresponding author at: Soft Robotics Research Center, Shenzhen Institute of Advanced Technology, Chinese Academy of Sciences, Shenzhen, 518055, Guangdong, China.
E-mail address: zy.xia@siat.ac.cn (Z. Xia).

https://doi.org/10.1016/j.jocs.2023.102083
Received 27 August 2022; Received in revised form 29 May 2023; Accepted 3 June 2023
Available online 9 June 2023

reduction methods depend on pre-computational snapshots of full-scale solutions of soft tissue deformation, increasing the computational cost and complexity. Therefore, how to achieve efficient dynamic modeling of soft tissue deformation is still an open problem.

Numerous works have been proposed for dynamic modeling of soft tissue deformation, including the finite element method and order reduction method. In the following, we review works related to dynamic modeling of soft tissue deformation.

The finite element methods have been typically developed for dynamic modeling of soft tissue deformation for decades [10,11]. A total Lagrangian explicit dynamics algorithm based on explicit time integration is proposed in [12] for computing deformation of soft tissue. In [13,14], deformation models using finite element method, Mass–Spring System or other models, with explicit, semi-implicit or implicit time integration, are used to calculate mechanical behaviors of deformable objects. In addition, GPU-based implementation is also incorporated to improve computational efficiency [15]. In our previous works [16,17], soft tissue deformation is computed using an implicit Euler method, which achieves relatively high computational efficiency and accuracy. Whereas simulation of soft tissue deformation using finite element methods with an implicit integration scheme achieve a high degree of accuracy, it is computationally intensive and complexities of soft tissue mechanics make it unsuitable for online oriented clinical scenes.

The order reduction methods have been proposed to achieve efficient and precise modeling of soft tissue deformation. A reduced order model is constructed through two sequential stages [18], i.e., construction of the reduced basis, and approximation of the nonlinear term. In the first stage, a sub-space spanned with the basis matrix of the state variable is constructed. The governing equation of the nonlinear problem is projected into a low dimension sub-space with a nonlinear term. After that, an approximation method is implemented to calculate the nonlinear term. The order reduction method has been widely used in the computational models of soft tissue deformation due to its computational efficiency [19–22]. The Proper Orthogonal Decomposition (POD) is one of the most popular methods to construct the reduced basis in the first stage of order reduction technique. In [19], the Proper Orthogonal Decomposition (POD) based order reduction method with explicit time integration was presented for surgical simulation. Yang et al. [23] developed the POD-based method to estimate cardiac conductivity. These methods can achieve efficient calculation of cardiac physiology, making them suitable for clinically oriented applications. Rama et al. [9] proposed an order reduction method called the Proper Orthogonal Decomposition with Interpolation (PODI) to simulate the heart, which drastically reduces the computation time. In the PODI-based approaches, the reduced basis is constructed from a set of parameter-dependent solutions of the full-order model, and the snapshots of the solution are approximated by minimizing error with the selection of the most important modes. Several techniques have been proposed to reduce the cost of evaluating nonlinear terms in order reduction methods, including the Empirical Interpolation Method (EIM). Chaturantabut et al. [24] proposed a discrete variant of EIM, known as Discrete Empirical Interpolation Method (DEIM), to effectively overcome the complexity of evaluating the nonlinear terms. Bonomi et al. [25] proposed a reduced framework based on matrix DEIM technique to simulate the cardiac contraction in which the coupled electro-mechanical problem was solved efficiently. Sipp et al. [26] compare the POD-Galerkin and POD-DEIM methods for nonlinear model reduction. The stability, accuracy and robustness, and appropriate quantitative measures of order reduction models are introduced and compared. Pagani et al. [27] propose to incorporate a k-means clustering in the state space of the snapshots into the approximation of the nonlinear terms in the order reduction method.

In the simulation of soft tissue, finite element method with hyperelastic material model and implicit time integration scheme was usually adopted to achieve relative high degree of accuracy, and effects were made to improve computational efficiency. In order reduced techniques, the main idea is to find a proper basis to project the dynamic system from a sub-space to the full-space. In POD-based methods of sub-space construction, basics functions are extracted from snapshots of soft tissue deformation. These methods have been successfully applied in computational model of soft tissue deformation, however, the main drawbacks are intensive offline computational cost and complexity. In EIM-based methods of nonlinear term estimation, pre-computation of soft tissue deformation with multi complex physiology and physics aspects increases the offline computational cost and complexity. Moreover, generation of representative snapshots of soft tissue deformation is a challenging task since environments and external manipulation applied on the soft tissue are usually complex. The handle-based reduced order models [28–30] provide a way to efficiently construct low-order subspace without the need for pre-computation of snapshots. Recent improvements are also presented to handle contact deformation using a learn-based method [31,32]. These methods also provide an opportunity for efficiently handling interaction between organs and surgical instruments in medical simulation. Hence, how to reduce computational cost and complexity is the major challenge in order reduction method for dynamic modeling of soft tissue deformation.

In this paper, a new Weighted Skinning and Cubature Integrated (WSC-integrated) order reduction method for dynamic modeling of soft tissue deformation is proposed. A weighted skinning integrated scheme is adopted to interpolate dynamic characterization of soft tissue, through which a sub-space is constructed conveniently. Internal elastic forces of soft tissue in reduced order sub-space are approximated using a cubature integrated scheme. Dynamics of soft tissue in this sub-space are then transformed back into the full-space. Simulation experiments and comparison show that the proposed order reduction method achieves efficient and accurate computation of soft tissue deformation.

The novelty of the presented work is to introduce WSC-integrated scheme into development of the new order reduction method for dynamic modeling of soft tissue deformation. The weighted skinning integrated scheme derived from handle-based reduced order method [33] is adopted to construct the sub-space, which provides accurate and convenient interpolation of soft tissue dynamics. In the meantime, a cubature integrated scheme [34] is adopted to calculate the elastic forces of soft tissue in the reduced order sub-space. The proposed method relies on integration schemes in both sub-space construction and internal forces estimation instead of pre-computed snapshots of soft tissue deformation. The proposed method is exempted from precomputing snapshots of soft tissue deformation, making it straightforward and easy to implement. This work provides efficient and accurate dynamic modeling of soft tissue deformation, which can further be adapted for patient-specific computation through parameters estimation. However, the selection strategy of samples for handles and elements could be further investigated.

The remainder of this paper is organized as follows. In Section 2, the concept of dynamic modeling of soft tissue deformation is briefly introduced. In Section 2.2, a new WSC-integrated order reduction method was proposed for dynamic modeling soft tissue deformation. Implementation and simulation results are shown in Section 3. A brief discussion is presented in Section 4.

2. Methods

2.1. Mechanical preliminary

In the presented dynamic modeling of soft tissue deformation, an finite element method is used to govern mechanical response of soft tissue. Deformation of soft tissue can be formulated as a function $\phi : \mathbb{R}^3 \rightarrow \mathbb{R}^3$, which maps the reference configuration to the current configuration. Material points of soft tissue in its reference state $\vec{X} \in \mathbb{R}^3$ move to the corresponding current state $\vec{x} = \phi(\vec{X}) \in \mathbb{R}^3$ under the

effects of physiological functions and external loads. The deformation gradient is used to characterize relative deformation of soft tissue, as

$$\boldsymbol{F} = \frac{\partial \phi(\vec{X})}{\partial \vec{X}} \tag{1}$$

The first Piola–Kirchhoff stress tensor can be obtained from derivation of strain energy function, as

$$\boldsymbol{P} = \frac{\partial W}{\partial \boldsymbol{C}} \frac{\partial \boldsymbol{C}}{\partial \boldsymbol{F}}, \quad \boldsymbol{C} = \boldsymbol{F}^T \boldsymbol{F} \tag{2}$$

where $\boldsymbol{C}$ is the right Cauchy Green tensor, and the strain energy function W is integration of energy density throughout the problem domain, as

$$W(\vec{x}; \vec{X}) = \int_{\Omega} \Psi(\boldsymbol{F}) d\Omega \tag{3}$$

In the presented work, a Mooney–Rivlin model is used to characterize elastic deformation of soft tissue. Other kinds of material models can also be incorporated. The strain energy density of Mooney–Rivlin material is as

$$\Psi(I_1, I_2) = \frac{1}{2}\mu_1[I_1 - 3] - \frac{1}{2}\mu_2[I_2 - 3] \tag{4}$$

where invariants of the right Cauchy Green tensor are given by

$$I_1 = tr\boldsymbol{C}, \quad I_2 = \frac{1}{2}(tr^2\boldsymbol{C} - tr\boldsymbol{C}^2) \tag{5}$$

In the dynamics model with finite element method, the geometry of soft tissue is discretized into tetrahedral meshes. Elastic forces generated in each tetrahedral mesh is calculated according the mechanical model as described in Section 2.1. Let $\boldsymbol{x} = (\vec{x}_0, \dots, \vec{x}_{n-1}) \in \mathbb{R}^{n\times 3}$ denotes position of vertices of the geometric mesh, where n is number of vertices. Since the elastic force is the negative gradient of the strain energy as $\boldsymbol{f} = -\partial W/\partial \boldsymbol{x}$, evolution of displacement $\boldsymbol{x}$ of mesh nodes is governed by the following equation:

$$\boldsymbol{M}\ddot{\boldsymbol{x}} = \boldsymbol{f}_e + \boldsymbol{f}_a \tag{6}$$

where $\boldsymbol{M}$ is the mass matrices, $\boldsymbol{f}_e$ is the elastic forces resulting from elastic deformation of soft tissue, and $\boldsymbol{f}_a$ is external load applied on soft tissue. In the presented work, the finite element method with an implicit time integration scheme is used to simulate soft tissue deformation. More details of the finite element method and the implicit time integration scheme have been presented in existing works [35,36].

2.2. WSC-integrated order reduction method

So far we have described dynamic modeling of soft tissue deformation using an finite element method in full-space. It allows to calculate the deformation of soft tissue with high degree of accuracy. However, this simulation method is computationally expensive, which limits its usage in online clinical scenes and requires high computational performance.

In the presented work, a new Weighted Skinning and Cubature Integrated (WSC-integrated) order reduced method is proposed to improve computational efficiency through reducing degrees of freedom in the dynamic modeling of soft tissue deformation, as stated in Eq. (6). The vertex positions $\boldsymbol{x} \in \mathbb{R}^{n\times 3}$ are represented in a reduced set of coordinates $\boldsymbol{q} \in \mathbb{R}^{4k\times 3}$, where an affine transform is used to project the coordinates from a sub-space to the full-space as

$$\boldsymbol{x} = \boldsymbol{U}\boldsymbol{q} \tag{7}$$

also the sub-space dimensions $4k \ll n$. The Eq. (6) can be rewrite as

$$\tilde{M}\ddot{\boldsymbol{q}} = \tilde{\boldsymbol{f}}_e + \tilde{\boldsymbol{f}}_b \tag{8}$$

where a tilde denotes reduced variables projected into the chosen sub-space: $\tilde{M} = \boldsymbol{U}^T\boldsymbol{M}\boldsymbol{U}$, and $\tilde{\boldsymbol{f}}_e = \boldsymbol{U}^T\boldsymbol{f}_e(\boldsymbol{U}\boldsymbol{q})$, $\tilde{\boldsymbol{f}}_a = \boldsymbol{U}^T\boldsymbol{f}_a(\boldsymbol{U}\boldsymbol{q})$ are mass matrix, elastic force, and external force in the reduced sub-space. In the deformation model with tetrahedral element, forces can be written as a sum of contributions over mesh elements $\mathcal{T}$:

$$\tilde{\boldsymbol{f}} = \sum_{e\in\mathcal{T}} U_e^T \boldsymbol{f}_e \tag{9}$$

where $\boldsymbol{f}_e$ is a 12-vector of forces for single tetrahedral element and U_e is a $12\times 4k$ sub-block of U for the respective element vertex.

Next, a new sub-space is constructed based on a weighted skinning integrated scheme and a cubature integrated scheme is incorporated to estimate internal elastic forces. The proposed method relies on integration schemes both in sub-space construction and internal elastic forces estimation instead of precomputed snapshots of soft tissue deformation. Since soft tissue dynamics are governed by a subspace with reduced coordinates, the computation burden of soft tissue deformation is significantly reduced.

2.3. Sub-space construction based on weighted skinning integrated scheme

In the proposed order reduction method, a set of skinning weights are used to construct a sub-space for the model order reduction, similar to the sub-space used in [33]. The furthest point sampling algorithm is incorporated to choose k sample handles $\boldsymbol{s}_j$ that distributes approximately equidistant over the mesh. Then radial basis functions around the handles are used to calculate preliminary weights for each vertex i with respect to the k handle. Specifically, the weights are defined as $\tilde{\boldsymbol{w}}_i = (B_{\boldsymbol{s}_1,r(\boldsymbol{q}_i)}, \dots, B_{\boldsymbol{s}_k,r(\boldsymbol{q}_i)})$, where r is a radius and $B_{\boldsymbol{y},r(\boldsymbol{x})} = b_r(d(\boldsymbol{x}-\boldsymbol{y}))$ is a scalar function related to mesh vertices. Finally, a normalization procedure is implemented as $\boldsymbol{w}_i = \tilde{\boldsymbol{w}}_i \cdot (1./\sum_j \tilde{w}_i^j)$ to ensure reproducibility of the rest shape.

In the skinning transformation, the position of mesh vertices is obtained via

$$\begin{pmatrix} \boldsymbol{x}_i^x \\ \boldsymbol{x}_i^y \\ \boldsymbol{x}_i^z \end{pmatrix} = \sum_{j=0}^{k} w_i^j \boldsymbol{A}_j \begin{pmatrix} \hat{\boldsymbol{x}}_i^x \\ \hat{\boldsymbol{x}}_i^y \\ \hat{\boldsymbol{x}}_i^z \\ 1 \end{pmatrix} \tag{10}$$

where $\boldsymbol{A}_j$ is k chosen as affine transformations (3×4 matrices) for each handle, w_i^j is weight and $\hat{\boldsymbol{x}} \in \mathbb{R}^{n\times 3}$ is rest position of the mesh vertices. From this, we can deduce a sub-space matrix

$$\boldsymbol{U} = (U_1 | \cdots | U_k) \tag{11}$$

$$U_j = \begin{pmatrix} w_0^j & \hat{\boldsymbol{x}}_0^x \cdot w_0^j & \hat{\boldsymbol{x}}_0^y \cdot w_0^j & \hat{\boldsymbol{x}}_0^z \cdot w_0^j \\ w_1^j & \hat{\boldsymbol{x}}_1^x \cdot w_1^j & \hat{\boldsymbol{x}}_1^y \cdot w_1^j & \hat{\boldsymbol{x}}_1^z \cdot w_1^j \\ \dots & & & \\ w_n^j & \hat{\boldsymbol{x}}_n^x \cdot w_n^j & \hat{\boldsymbol{x}}_n^y \cdot w_n^j & \hat{\boldsymbol{x}}_n^z \cdot w_n^j \end{pmatrix} \tag{12}$$

and entries of the affine transformations can be interpreted as sub-space coordinates

$$\boldsymbol{q} = (\boldsymbol{A}_0^T, \dots, \boldsymbol{A}_{k-1}^T)^T \tag{13}$$

Then, the transformation can be concisely written as described in Eq. (7). After that, we can project the coordinates from the sub-space to its full-space in dynamic modeling of soft tissue deformation.

2.4. Internal force estimation based on Cubature integrated scheme

In the presented work, a cubature integrated scheme is incorporated to evaluate the internal elastic forces, where the forces are projected from the sub-space to the full-space. The scheme works by observing that elastic strain energy $E(\boldsymbol{q})$ and internal forces $\tilde{\boldsymbol{f}}$, for reduced coordinates $\boldsymbol{q}$, are obtained by integrating the energy density $\Psi(X, \boldsymbol{q})$, and its gradient over the entire mesh, as

$$\tilde{\boldsymbol{f}} = \int_{\Omega} \frac{\partial \Psi(X, \boldsymbol{q})}{\partial \boldsymbol{q}} d\Omega \tag{14}$$

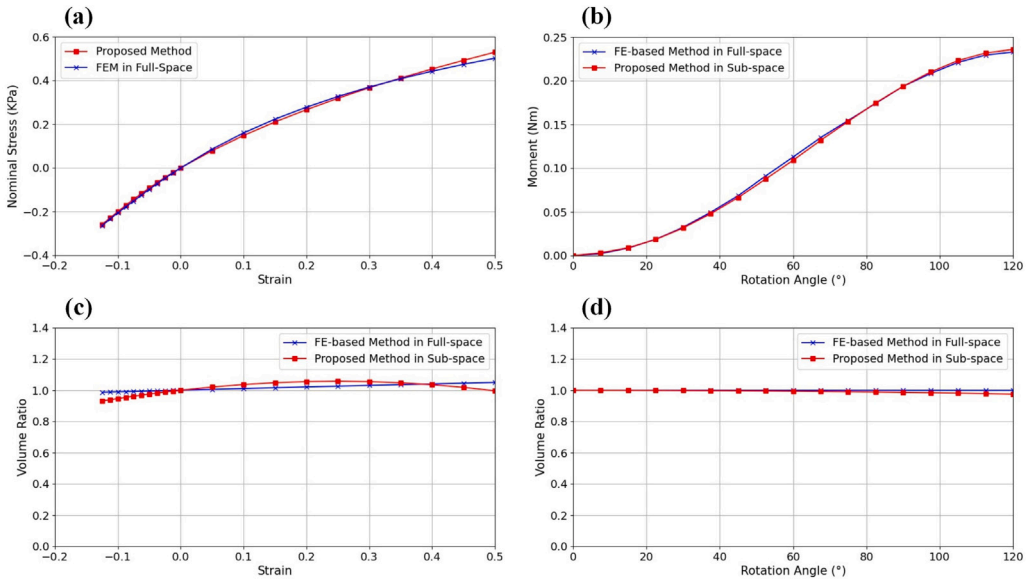

Fig. 1. The results of both normal deflection and volumetric responses of the soft matter to uniaxial tensile and twist tests. Both results of the finite element method in full-space and our method are presented. (a) Strain–stress relationship. (b) Evolution of the moment with respect to the rotation angle. (c) Volumetric responses with respect to the strain. (d) Volumetric responses with respect to the rotation angle.

As proposed in [37], we approximate the integration in Eq. (14) using a k'-elements cubature integrated scheme, instead of evaluating $\tilde{\boldsymbol{f}}$ using the exact formula $\tilde{\boldsymbol{f}} = \boldsymbol{U}^T \boldsymbol{f}(\boldsymbol{U}\boldsymbol{q})$. To achieve this, we determine k' sampling elements, such that

$$\tilde{\boldsymbol{f}}(\boldsymbol{q}) = \int_{\Omega} \frac{\partial \Psi(X, \boldsymbol{q})}{\partial \boldsymbol{q}} d\Omega \approx \sum_{i=1}^{k'} \alpha_i \boldsymbol{g}(X_i, \boldsymbol{q}) \tag{15}$$

where $\alpha_i \in \mathbb{R}$ is a scalar cubature weight applied to sample i, and $\boldsymbol{g}(X_i, \boldsymbol{q})$ is "reduced-force density" as

$$\boldsymbol{g}(X_i, \boldsymbol{q}) = -\nabla_{\boldsymbol{q}} \Psi(X, \boldsymbol{q}) = U_i^T \boldsymbol{f}_i(U_i \boldsymbol{q}) \tag{16}$$

where $U_i \in \mathbb{R}^{12\times 4k}$ is rows of U that correspond to vertices of tetrahedron i, and $\boldsymbol{f}_i$ is material forces on vertices of the ith tetrahedron that is calculated using element-sampled version of the material force function.

Sampling elements. During the construction of internal force sub-space, k' approximately equidistant sample elements on the geometrical mesh are chosen. After that, weight function α_j with a limited support domain around each of the samples is constructed. Radial basis functions around the sampled element are then used to calculate the initial weights for each tetrahedrons and each of the k' sample. Since linear tetrahedral elements are used to discretize the geometrical mesh of soft tissues in the discrete cubature integrated scheme, force density remains constant over each element.

Computing weights. Given a set of sampled tetrahedrons, the weight functions are then interpolated to calculate the cubature weights $\boldsymbol{\alpha} = (\alpha_0, \ldots, \alpha_i, \ldots, \alpha_{k'})$, and then normalized to sum to one of each element. Similar to [34], we construct an interpolation scheme for the elastic energy based on biharmonic generalized barycentric coordinates (BGBC). The cubature weights are derived by integrating the basis functions of the interpolation scheme. The implicit assumption in this construction is that the transformations of the soft tissue deformation vary smoothly across the mesh. In the BGBC based interpolation, the elastic energy density $\Psi(\boldsymbol{X})$ can be integrated as

$$\Psi(\boldsymbol{X}) = \sum_j \alpha_j(\boldsymbol{X}) \Psi(\boldsymbol{X}_j) \tag{17}$$

The full energy W can be computed by integrating the interpolated energy density on the entire reference shape:

$$W = \int_{\Omega} \sum_j \alpha_j(\boldsymbol{X}) \Psi(\boldsymbol{X}_j) d\Omega = \sum_j \left(\int_{\Omega} \alpha_j(\boldsymbol{X}) d\Omega \right) \Psi(\boldsymbol{X}_j) \tag{18}$$

Based on the integration scheme above, the cubature weights can be obtained by integrating the BGBC on the reference configuration, as following:

$$w_j = \int_{\Omega} \alpha_j(\boldsymbol{X}) d\Omega \tag{19}$$

It is able to approximate the energy well and is also relatively fast.

3. Results

In this section, we will evaluate the accuracy and efficiency of the proposed method. We computed the deformation of soft tissue using the proposed order reduction method and compared the results with an finite element method [38,39] in full-space using implicit time stepping. The simulation experiments are implemented using a C++ program. In order to demonstrate the potential usage of the proposed method, simulation of left ventricle dynamics is presented. We perform the simulation on Intel(R) Xeon(R) E5-1603 v3 CPU.

3.1. Accuracy comparison and analysis

Simulation experiments of a cubical model with uniaxial tensile and twist tests are conducted. Boundary condition is applied by prescribing displacements on the selected vertices. At the end of each simulation step, the vertices at the left end of the cubical model are fixed by setting displacements to zero, tensile and twist are applied to the cubical model by setting the displacements of vertices at the right end of the cubical model to specified values. As shown in Fig. 1, both deformation and volumetric responses during the tests are presented. Stress with respect to strain, moment with respect to rotation angle and volume ratio are calculated using the proposed method and an finite element method in full-space. The nominal stress is calculated based on the elastic force over the nodes on the right side face and the cross-sectional area of the cuboid model. The strain is calculated based on the ratio of tensile to length of the cuboid model. Compared with the results of the finite element method in full-space, relative root mean square error

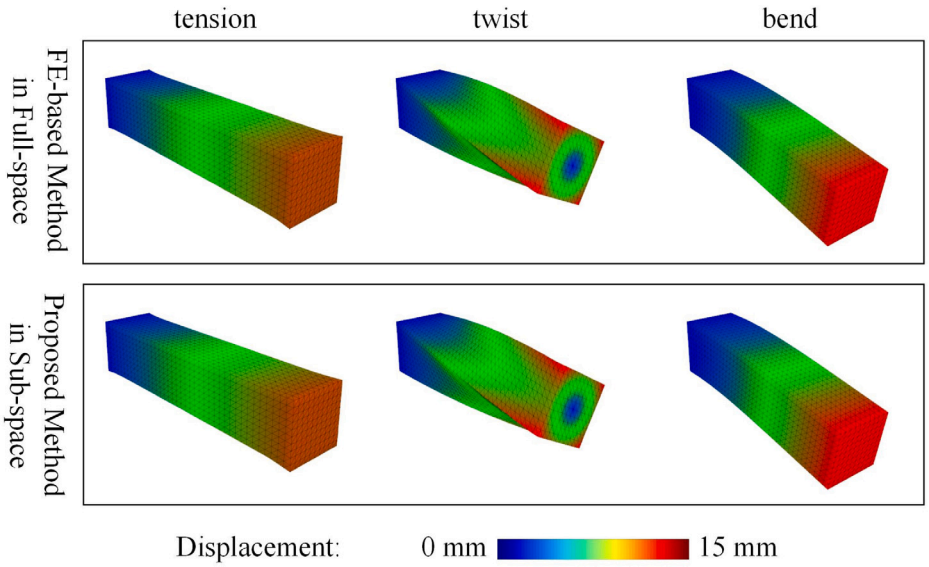

Fig. 2. The visual results of the deformation tests. Displacement of the cubical model are rendered with color maps.

(RMSE) of the proposed method is 4.27%, 3.11%, 2.15%, and 2.63% for strain–stress relationship, strain-volume relationship, rotation-moment relationship, and rotation-volume relationship, respectively. Moreover, there are no distinctive visual differences between cubical model deformation computed using the proposed method and the finite element method in full-space, as shown in Fig. 2. The relative RMSE for displacement of cubical model computed using the proposed method ranges from 3.06% to 5.84%. Simulation results show that a high degree of qualitative consistency between the proposed method and the finite element method in full-space. Furthermore, as a non-linear material model is incorporated, simulation results of soft tissue deformation act non-linearly, as shown in Fig. 1. The cubical model (2 cm $*$ 2 cm $*$ 8 cm) contains 7273 vertices and 37 592 tetrahedrons. The material parameters of the cubical model are set as follows: mass density ρ = 500 kg/m^3, $\mu_1 = 0.5$ kPa and $\mu_2 = 0.6$ kPa. There are 250 sample handles used to construct a sub-space and 3000 elements used to estimate the internal elastic forces.

Next, in order to evaluate accuracy of the proposed model with different choice of sub-space and cubature integrated scheme, we perform simulation tests on cubical model with different number of sample handles and elements. As shown in Table 1, the number of sample handles ranges from 74 (counts for 1.0% of all vertex) to 364 (counts for 5.0% of all vertex), and the number of sample elements ranges from 1880 (counts for 5.0% of all elements) to 2820 (counts for 7.5% of all elements). The relative RMSE of soft tissue deformation computed using the proposed method with respect to the finite element method in full-space are ranges from 21.82% to 2.29%. Simulation results show that accuracy of the proposed method increases with increase in sample handles. Furthermore, accuracy of the proposed method is lower as 6.25% of elements were incorporated into estimation of internal elastic force. That is because the under-fitting of internal forces occurs when the sampled elements are too few, while the over-fitting of internal forces happens when the number of sampled elements is too high [37]. In order to better demonstrate accuracy of the proposed method, experiments of soft tissue deformation with varying resolution are presented in Appendix B. Overall, with proper selecting of sample handles and elements, the proposed method achieves comparable accuracy to the finite element method in full-space.

3.2. Efficiency comparison and analysis

To demonstrate the efficiency performance of the proposed method, we perform simulation tests on a set of soft tissue models with proper selection of sample handles and elements. As shown in Table 2, geometrical model with vertices (range from 3315 to 7273) and elements (range from 15 810 to 170 487) are simulated with the proposed method. In our proposed method, the computation time ranges from 6.07 ms to 19.31 ms, while in the finite element method, it ranges from 288.98 ms to 688.83 ms in full space. Experiments show that the computation time of the proposed method slightly increases as the number of vertices increases. The proposed method achieves a higher degree of computational efficiency compared to the finite element method in full-space.

Next, to further assess the performance of the proposed method, we compare the average one-step calculation time between our developed method and the finite element method in full-space. As shown in Table 1, the cubical model with 7273 vertices and 37 592 tetrahedrons is used in the experimental test. Each time step requires 10.07 ms - 21.22 ms to calculate deformation of soft tissue for our developed method with different selection of sample handles. We perform experiments using the finite element method in full-space, which requires 688.83 ms in each time step. Our method achieves high degree of efficiency with proper selection of sample handles and elements. When number of sample elements is 2350 (counts for 6.25% of all elements), the proposed method takes approximately 1/54 to 1/37 amount of computation time compared with the finite element method in full-space.

In the proposed method, additional procedures, including computation of skinning and cubature weights, are needed before the simulation of soft tissue deformation. Sampling-related algorithms, that significantly reduce the computation burdens of deformation simulation, are incorporated into our developed method. Moreover, these weight parameters can be reused and these additional procedures can be conducted when constructing the geometrical mesh of soft tissue. These features of the proposed method enable efficient simulation of soft tissue deformation in online clinical scenes.

3.3. Dynamics of left ventricle with order reduction method

We implement the proposed order reduction method for the simulation of left ventricle dynamics. The geometrical mesh of left ventricle is reconstructed from cardiac magnetic resonance images. The left ventricle deforms under the effect of myocardium contraction and blood flow in a cardiac cycle. Finally, simulation results of left ventricle deformation is presented.

Table 1
Deformable objects and their computational results. The cubical model (2 cm ∗ 2 cm ∗ 8 cm) contains 7273 vertices and 37 592 tetrahedrons. There are 1880 (5.0%) to 2820 (7.5%) elements sampled for estimation of internal elastic forces.

Number of sample handles (Sampling ratio)	Number of sample elements (Sampling ratio)	Relative error (%)	Computation time (ms)
74 (1.0%)	1880 (5.0%)	21.82	10.70
108 (1.5%)	1880 (5.0%)	15.80	12.00
150 (2.0%)	1880 (5.0%)	16.42	12.18
180 (2.5%)	1880 (5.0%)	16.11	12.73
220 (3.0%)	1880 (5.0%)	10.31	13.25
250 (3.5%)	1880 (5.0%)	5.59	13.87
290 (4.0%)	1880 (5.0%)	3.90	15.11
327 (4.5%)	1880 (5.0%)	3.38	15.42
364 (5.0%)	1880 (5.0%)	2.59	15.75
74 (1.0%)	2350 (6.25%)	8.60	12.82
108 (1.5%)	2350 (6.25%)	5.43	13.82
150 (2.0%)	2350 (6.25%)	4.90	14.08
180 (2.5%)	2350 (6.25%)	5.97	14.28
220 (3.0%)	2350 (6.25%)	4.44	15.48
250 (3.5%)	2350 (6.25%)	4.99	15.80
290 (4.0%)	2350 (6.25%)	3.31	16.69
327 (4.5%)	2350 (6.25%)	2.55	17.81
364 (5.0%)	2350 (6.25%)	2.29	18.41
74 (1.0%)	2820 (7.5%)	11.24	14.51
108 (1.5%)	2820 (7.5%)	6.17	15.45
150 (2.0%)	2820 (7.5%)	6.26	15.75
180 (2.5%)	2820 (7.5%)	9.66	16.17
220 (3.0%)	2820 (7.5%)	7.47	17.33
250 (3.5%)	2820 (7.5%)	4.05	18.01
290 (4.0%)	2820 (7.5%)	5.64	18.63
327 (4.5%)	2820 (7.5%)	3.16	19.49
364 (5.0%)	2820 (7.5%)	2.48	21.22

Table 2
Assessment of efficiency of the proposed method. A set of soft tissue models are incorporated.

Mesh vertices (Sampling handles)	Mesh elements (Sampling elements)	Relative error (%)	Computation time of finite element method in full-space (ms)	Computation time of our method in sub-space (ms)
7273 (300)	170 487 (3000)	4.74	688.83	19.31
4265 (150)	21 009 (1500)	2.88	413.50	9.89
3266 (100)	15 924 (1000)	2.32	296.59	6.17
3315 (100)	15 810 (1000)	1.26	288.98	6.07

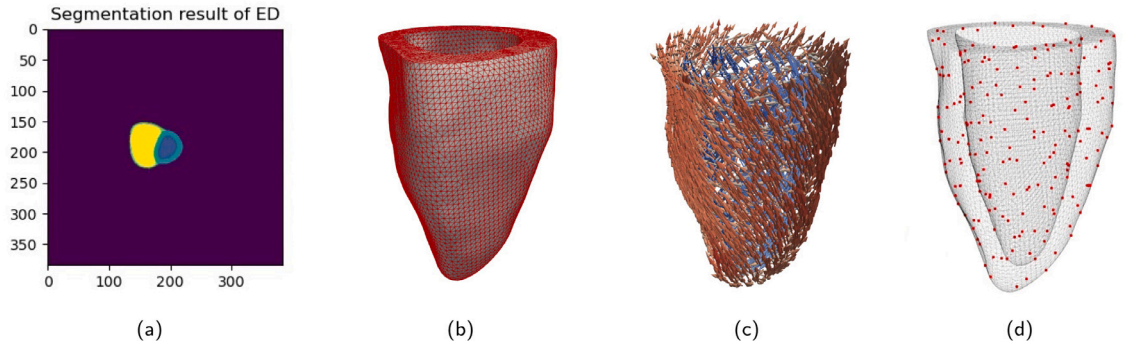

Fig. 3. Preprocess of the CMR images: (a) segmentation of the ventricular at the end-diastole. (b) the finite element mesh of a left ventricle geometry reconstructed from the segmentation results. (c) the myocardial fiber orientation assigned using the LDRB algorithm [40]. (d) sampling handles in the simulation of left ventricle dynamics based on the proposed order reduction method, which are used to construct the sub-space.

Data and preprocessing. Cardiac magnetic resonance (CMR) images from the Automated Cardiac Diagnosis Challenge (ACDC) [41] are used to construct the geometries of left ventricle. There are 17 777 nodes and 70 481 tetrahedral elements in the left ventricle mesh. In order to characterize anisotropic properties and active stress of myocardium, orientation of fiber, sheet, and sheet normal are identified. The Laplace Dirichlet Rule-Based (LDRB) algorithm proposed by Finsberg et al. [40] is used to assign rule-based fibers of myocardium. The angle on endocardium and epicardium are +60° and −60°, respectively. Fig. 3 shows the segmentation results of CMR images, the three-dimensional mesh reconstructed, the fibers of myocardium, and sampling handles of left ventricle. Material parameters of the myocardium refers to the existed work [42,43], as mass density $\rho = 1265\ \mathrm{kg/m^3}$, $\mu_1 = 2.1$ kPa and $\mu_2 = 0$.

Simulation of left ventricle dynamics. In a cardiac cycle, the left ventricle deforms under the effect of myocardium contraction and blood flow. In the presented simulation of left ventricle dynamics, the entire cardiac cycle is divided into four stage: isochoric contraction for systole;

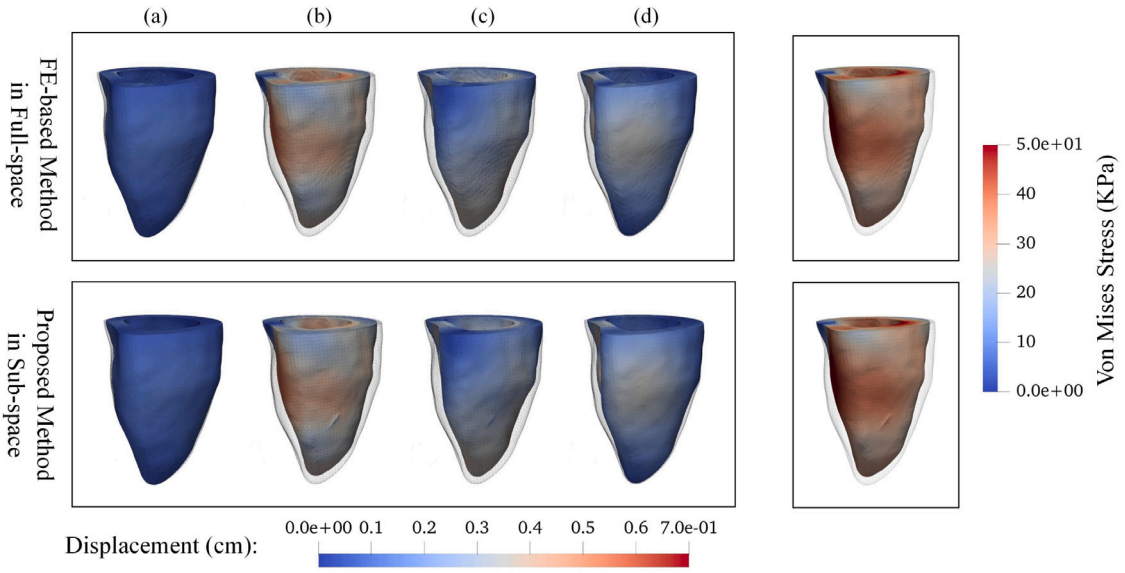

Fig. 4. Snap shots of the solutions (displacements and stress) of left ventricle dynamics in a cardiac cycle. The proposed order reduction method is used to govern the of left ventricle dynamics, as described in Section 2.2. (a)–(d) refer to different stage of the cardiac cycle. Von Mises stress of myocardium during stage (b) are also presented.

ejection during systole; isochoric relaxation for diastole; and filling during diastole, as followed [44]. As shown in Fig. 3(d), there are 300 sample handles were chosen to construct the sub-space. The sub-space matrix is pre-computed and stored for simulation of left ventricle dynamics. In the cubature sampling scheme, 3600 elements approximately equidistant distributed in the left ventricle mesh are chosen. Finally, dynamics of left ventricle is simulated using the proposed order reduction method. In each phase, the active forces generated by myocardium in cubature sampling elements are calculated. The forces generated by blood pressure are imposed on the surface are treated as constant in the simulation step, which can be easily transformed into the sub-space.

Simulation results and comparison. Simulation results of left ventricle dynamics based on the proposed order reduction method are shown in Fig. 4. In the first phase, cavity pressure increases due to active contraction of myocardium, while cavity volume remains constant. After that, blood in left ventricle is pumped into the aortic, leading to decrease the cavity volume. During isochoric diastole phase, myocardium starts to relax and the cavity pressure decreases to minimum. During the filling phase of diastole, blood fills left ventricle and both the cavity pressure and volume increase slightly. It takes 21.81 ms to solve the reduced order system equation in each simulation step. Conversely, the simulation of left ventricle dynamics using finite element method in full-space which takes 932.35 ms in each simulation step, which achieves an improvement of approximately 43 times during online stage. Difference between their results is negligible (with relative RMSE of 2.4%). Efficient and accurate modeling of left ventricle dynamics can be achieve based on the proposed method, which can be further incorporated for clinical application for disease diagnosis and treatment.

4. Discussion

In this paper, a WSC-integrated order reduction method for dynamic modeling of soft tissue deformation is presented for engineering assistive medical procedures. The deformation of soft tissue is transformed into a sub-space with a weighted skinning integrated scheme, and the internal elastic forces are estimated through a cubature integrated scheme. The proposed method achieves efficient and accurate dynamic modeling of soft tissue deformation because it takes advantage of simplicity of the skinning weight integrated scheme and efficiency of the cubature integrated scheme. When constructing the sub-space, the skinning weight integrated scheme uses a radial basis functions to calculate the weight of deformation between the handles and vertices, hence building an approximate mapping between the sub-space and the full-space. This integrated-based scheme is exempted from pre-computing snapshots of soft tissue deformation in full-space and consumes less computational resources. In addition, another mapping methods between handles and vertices, such as projective skinning [45] and neural network [46], can also be incorporated into constructing the sub-space in the presented work. The handle-based reduced order model is one of the effective ways to construct a low order subspace, which has been widely used in the field of Computer Graphics, including rig space dynamics [47], frame-based elastic models [29], cage-based deformations [48], and other handle-based methods
[28–30,49]. The key ideas behind these methods for subspace construction lie on the following two aspects: (1) find proper transformation between displacement of handles and deformation of soft objects; and (2) govern dynamic of soft objects within low order space. For example, in hyper-reduced projective dynamics [30], a subspace is created from skinning weights with RBFs and a constraint projection fitting method is incorporated to reduce computation expense, which is similar to our presented work. In complementary dynamics [49], displacements of handles are transformed into deformation of soft objects, while *additional* complementary displacements are calculated based on inherent dynamics mechanics of soft objects. These methods have been demonstrated to be effective ways to reduce order of dynamic models of soft tissue, which could be used in medical simulation in future. The other aspects of our proposed method is estimating the internal elastic forces. The cubature integrated scheme is incorporated. It achieves efficient estimation of internal elastic forces of soft tissue in the online stage. The proposed method is computational efficient both in the online and offline stage, which makes it suitable for online clinical scenes. Moreover, compared with the low-order mathematical model of soft tissue organs [50,51], deformation of soft tissue with precise anatomical details can be characterized based on the proposed method. It is suitable for dynamic modeling of soft tissue organs that presents complex physiology and physics aspects.

In the dynamic modeling of soft tissue deformation, accuracy and efficiency are the two major aspects of performance and assessment metrics [52,53]. Various choices of material model (linear elastic vs.

hyper-elastic), spatial discretization and time integration schemes (explicit integration vs. implicit integration) leads to different performance of accuracy and efficiency [54]. Finite element method with hyper-elastic material model and implicit time integration scheme presents relative high degree of accuracy, but relative low degree of efficiency, which is usually applied in medical simulation [55,56]. In this work, we chose finite element method with a hyper-elastic material model and an implicit time integration scheme as benchmark, and compared it to our proposed method. The implementation and source code [38] of the finite element method, as well as its verification results [39], have been reported in existing works. The implicit time integration scheme is based on the Backward Euler method and is unconditionally stable [35,36]. An iterative method is employed to solve the underlying system equations resulting from the deformation model. The iterative process terminates when the residual decreases to a desired threshold, or after exceeding a maximum number of iterations [35,57]. There are numerous works [14,15,17] and open-source codes [13,38,58] which use the finite element method with implicit time integration schemes to achieve accurate simulation of soft tissue deformation. Boundary conditions are usually applied by prescribing displacements on the selected vertices in the end of each simulation steps. Experimental results show that the proposed method achieves comparable accuracy to the finite element methods and real-time performance. Moreover, compared with existing order reduction methods, our proposed method does not require pre-computation of snapshots of soft tissue deformation, which is a challenging task in medical scene.

Various kinds of materials models have been proposed to characterize constitutive behaviors of soft tissue, including Ogden material model, Mooney–Rivlin material model, Neo-Hookean material model, etc [59,60]. More experiments with different material models have been performed to demonstrate the flexibility of the proposed method, as shown in Appendix A. However, for perfectly incompressible and nearly incompressible continuum (with high Poisson's ratio), volumetric locking [61] can occur in simulation of deformation using a finite element method. In the presented work, we focus on order reduction method for soft tissue simulation, and countermeasures against volumetric locking are not take into account. Experimental tests were conducted with different mesh resolutions, as shown in Appendix B. Experiment results show a small variation of the volume ratio and no significance decrease in stiffness as the meshes were refined. Existing works [62] also report using Poisson ratios of no more than 0.45 in order to alleviate locking artifacts. However, limitations still exist in the proposed method due to disregarding the volumetric locking phenomenon. Incompressibility constraints to the tetrahedral element would result in an increase of stiffness, especially for continuum with high Poisson's ratio. Convergence studies on the mesh resolution may reveal an increase in accuracy and decrease in numerical stiffness, yet locking may still occur [63]. On the other hand, small Poisson's ratio could alleviate locking artifacts at the cost of losing physical accuracy [64]. Countermeasures are expected to circumvent volumetric locking issue thoroughly [63]. In the proposed method, the construction of subspace and estimation of internal elastic force are independent of the spatial discretization scheme. A specifically designed tetrahedral element [65,66] can be employed to avoid the volume locking issue.

However, the proposed order reduction method for dynamic modeling of soft tissue deformation has some limitations that should be investigated further as follows: (a) how to optimize the algorithm of choosing the sampling handles and elements. An iterative search algorithm is used in our work to find the sampling handles and elements that are approximately equidistant distributed in the geometrical mesh of soft tissue. However, the accuracy of the proposed method drops due to over-fitting when 7.5% of the elements are selected, compared to 6.25%. An improved algorithm might be investigated to increase the accuracy and stability of the simulation. Several works have been proposed to generate handles for the handle-based order reduction method [67,68]. These works may provide an opportunity to optimally choose the sampling handles and elements during construction of geometrical mesh of the soft tissue. (b) countermeasures against volumetric locking. There are numerous works on finite element methods [64,69,70] and order reduction methods [19,71], in which the volumetric locking issue is addressed. In this presented work, the simulation results of our method and the finite element method do not consider the issue of volumetric locking. Therefore, further investigation on volumetric locking within order reduction methods should be conducted in future works.

CRediT authorship contribution statement

Wenguo Hou: Conceptualization, Methodology, Investigation, Software, Visualization, Writing – original draft. **Jing Xiong:** Methodology, Writing – review & editing. **Zeyang Xia:** Conceptualization, Methodology, Supervision, Writing – review & editing.

Declaration of competing interest

The authors declare that they have no known competing financial interests or personal relationships that could have appeared to influence the work reported in this paper.

Data availability

No data was used for the research described in the article.

Acknowledgments

This work does not concern any ethical issue. This work was supported by the National Natural Science Foundation of China (U2013205, 61773365, 62103402), and in part by the Chinese Academy of Sciences Youth Innovation Promotion Association Excellent Member Program (Y201968), and Guangdong Basic and Applied Basic Research Foundation, China under Grant 2022B1515020042, and Shenzhen Science and Technology Program, China under Grants JCYJ20220818101603008 and China Postdoctoral Science Foundation (2021M703387). We confirm that there are no known conflicts of interest associated with this publication and there has been no significant financial support for this work that could have influenced its outcome.

Appendix A. Experiments of soft tissue deformation with different material models

In computational models of soft tissue deformation, there are lot of material models are used to characterize elastic response to soft tissues, including Ogden model, Mooney–Rivlin model, Neo-Hookean model, etc. In this paper, a new order reduction method was proposed for dynamic modeling of soft tissue deformation. In the developed method, construction of subspace and estimation of internal elastic force are independent of the material models, which means that the method is compatible with different soft material models. In the presented work, Mooney–Rivlin model is picked as an example. A variety of material models are used to demonstrate flexibility of the proposed method.

In the presented simulation experiments, a cubical model (2 cm $*$ 2 cm $*$ 8 cm) contains 7273 vertices and 37 592 tetrahedrons are incorporated. There are 250 sample handles used to construct a subspace and 3000 elements used to estimate the internal elastic forces. Both the Ogden model, Mooney–Rivlin model, Neo-Hookean model and linear elastic model are incorporated. The material parameters of the cubical model are set as follows: mass density $\rho = 500\ \mathrm{kg/m^3}$, $\mu_1 = 0.5$ kPa and $\mu_2 = 0.6$ kPa for Mooney–Rivlin model; mass density $\rho = 500\ \mathrm{kg/m^3}$, Young's modulus of $10^8\ \mathrm{N/m^2}$, and Poisson ratio of 0.4 for Neo-Hookean model; mass density $\rho = 500\ \mathrm{kg/m^3}$, Young's modulus of $10^8\ \mathrm{N/m^2}$, and Poisson ratio of 0.4 for StVK model. Simulation results are as shown in Fig. 5. Simulation results with different models demonstrate the flexibility of the proposed method.

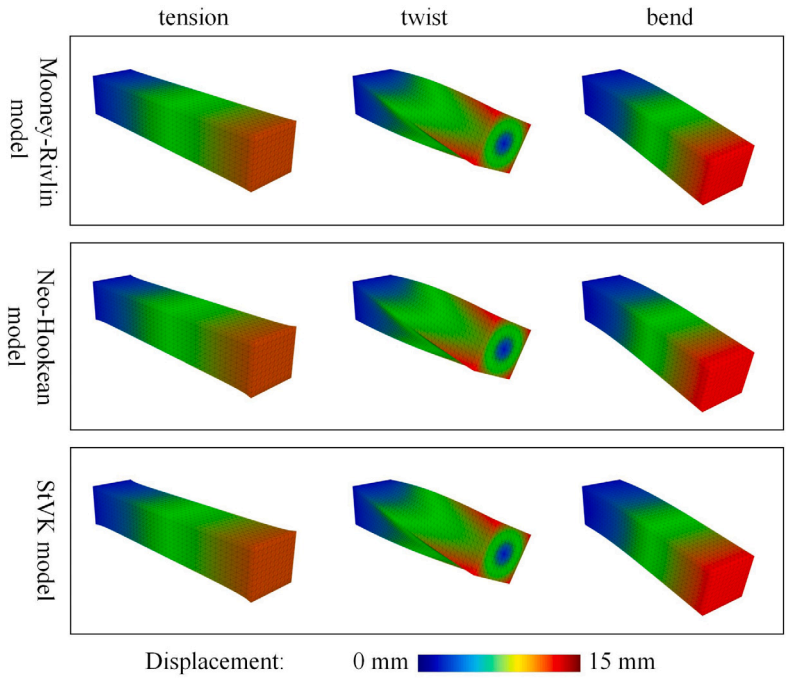

Fig. 5. The visual results of the deformation tests with different material models. Displacement of the cubical model are rendered with color maps.

Table 3
Deformable objects with varying resolution and their computational results. The cubical model (2 cm ∗ 2 cm ∗ 8 cm) contains 2519 vertices and 12 499 tetrahedrons for low resolution, 9284 vertices and 43 517 tetrahedrons for high resolution. The relative RMSE of soft tissue deformation computed using the proposed method with respect to the finite element method in full-space.

Low resolution				High resolution			
Number of sample handles (Sampling ratio)	Number of sample elements (Sampling ratio)	Relative error (%)	Computation time (ms)	Number of sample handles (Sampling ratio)	Number of sample elements (Sampling ratio)	Relative error (%)	Computation time (ms)
50 (2.0%)	650 (5.0%)	13.95	8.31	185 (2.0%)	2176 (5.0%)	11.05	28.09
63 (2.5%)	650 (5.0%)	9.42	8.12	232 (2.5%)	2176 (5.0%)	11.73	39.82
75 (3.0%)	650 (5.0%)	10.05	9.11	278 (3.0%)	2176 (5.0%)	7.30	48.38
88 (3.5%)	650 (5.0%)	7.28	10.74	325 (3.5%)	2176 (5.0%)	5.33	37.90
101 (4.0%)	650 (5.0%)	5.03	11.84	371 (4.0%)	2176 (5.0%)	3.70	43.35
113 (4.5%)	650 (5.0%)	3.96	10.92	418 (4.5%)	2176 (5.0%)	2.55	48.48
126 (5.0%)	650 (5.0%)	4.92	12.57	462 (5.0%)	2176 (5.0%)	2.77	63.41
50 (2.0%)	815 (6.25%)	6.99	9.92	185 (2.0%)	2720 (6.25%)	9.57	49.43
63 (2.5%)	815 (6.25%)	5.27	10.30	232 (2.5%)	2720 (6.25%)	8.98	42.00
75 (3.0%)	815 (6.25%)	7.78	10.47	278 (3.0%)	2720 (6.25%)	6.77	46.38
88 (3.5%)	815 (6.25%)	4.68	12.13	325 (3.5%)	2720 (6.25%)	4.74	51.52
101 (4.0%)	815 (6.25%)	1.93	12.86	371 (4.0%)	2720 (6.25%)	3.92	55.35
113 (4.5%)	815 (6.25%)	2.66	13.85	418 (4.5%)	2720 (6.25%)	2.35	52.66
126 (5.0%)	815 (6.25%)	2.10	15.28	462 (5.0%)	2720 (6.25%)	2.89	64.34
50 (2.0%)	875 (7.5%)	5.72	9.29	185 (2.0%)	3264 (7.5%)	9.53	44.06
63 (2.5%)	875 (7.5%)	4.59	10.81	232 (2.5%)	3264 (7.5%)	7.35	39.70
75 (3.0%)	875 (7.5%)	4.33	10.76	278 (3.0%)	3264 (7.5%)	6.67	46.17
88 (3.5%)	875 (7.5%)	2.94	11.36	325 (3.5%)	3264 (7.5%)	4.11	57.66
101 (4.0%)	875 (7.5%)	2.26	12.82	371 (4.0%)	3264 (7.5%)	3.04	63.88
113 (4.5%)	875 (7.5%)	3.87	13.44	418 (4.5%)	3264 (7.5%)	2.51	65.38
126 (5.0%)	875 (7.5%)	2.27	14.45	462 (5.0%)	3264 (7.5%)	2.06	91.60

Appendix B. Experiments of soft tissue deformation with varying resolution

The cubical model (2 cm ∗ 2 cm ∗ 8 cm) in these experimental tests is with the same size as the one in Section 3.1, but with a different resolution. Uniaxial tensile is conducted on the cubical model and deformation during the tests is computed and compared with the finite element method in full-space. As shown in Table 3, experimental results show that the proposed method achieves a relative high degree of accuracy and real-time performance. Compared with simulation results in Table 1, it achieves a similar degree of accuracy with varying resolution. In the experimental results of the finite element method with different mesh resolution, the nominal stresses regard to strain of 0.3 are 0.371 kPa (low resolution), 0.370 kPa (medium resolution) and 0.368 kPa (high resolution), and the volume ratios are 1.032 (low resolution), 1.031 (medium resolution) and 1.031 (high resolution), respectively. In the experimental results of the proposed order reduction method with different mesh resolution (sampling ratio for handles and elements are 3.0% and 6.25%, respectively), the nominal stresses regard to strain of 0.3 are 0.367 kPa (low resolution), 0.366 kPa (medium resolution) and 0.363 kPa (high resolution), and the volume ratios are 1.054 (low resolution), 1.055 (medium resolution) and 1.055 (high resolution), respectively. A small variation of the volume ratio and no significance decrease in stiffness were observed. In simulation

of soft tissue deformation for clinical scene, geometrical models with high resolution can characterize anatomical details of organs better, but require more computation expense. Trade-offs in terms of speed and details should be made when constructing the geometrical model and low order space for simulation.

References

[1] S.A. Niederer, J. Lumens, N.A. Trayanova, Computational models in cardiology, Nat. Rev. Cardiol. 16 (2019) 100–111.

[2] B. Stojanovic, M. Svicevic, A. Kaplarevic-Malisic, R.J. Gilbert, S.M. Mijailovich, Multi-scale striated muscle contraction model linking sarcomere length-dependent cross-bridge kinetics to macroscopic deformation, J. Comput. Sci. 39 (2020) 101062.

[3] S. Li, B. Chopard, J. Latt, Continuum model for flow diverting stents in 3D patient-specific simulation of intracranial aneurysms, J. Comput. Sci. 38 (2019) 101045.

[4] K. El-Monajjed, M. Driscoll, Haptic integration of data-driven forces required to gain access using a probe for minimally invasive spine surgery via cadaveric-based experiments towards use in surgical simulators, J. Comput. Sci. 60 (2022) 101569.

[5] J. Xiong, C. Xu, K. Ibrahim, H. Deng, Z. Xia, A mechanism-image fusion approach to calibration of an ultrasound-guided dual-arm robotic brachytherapy system, IEEE/ASME Trans. Mechatronics 26 (2021) 3211–3220.

[6] H. Finsberg, G. Balaban, S. Ross, T.F. Håland, H.H. Odland, J. Sundnes, S. Wall, Estimating cardiac contraction through high resolution data assimilation of a personalized mechanical model, J. Comput. Sci. 24 (2018) 85–90.

[7] A.S. Ponukumati, X. Wu, P.W. Kahng, J. Skinner, J.A. Paydarfar, R.J. Halter, A system for characterizing intraoperative force distribution during operative laryngoscopy, IEEE Trans. Biomed. Eng. 67 (2020) 2616–2627.

[8] N. Lauzeral, D. Borzacchiello, M. Kugler, D. George, F. Chinesta, A model order reduction approach to create patient-specific mechanical models of human liver in computational medicine applications, Comput. Methods Programs Biomed. 170 (2019) 95–106.

[9] R.R. Rama, S. Skatulla, Towards real-time modelling of passive and active behaviour of the human heart using PODI-based model reduction, Comput. Struct. 232 (2020) 105897.

[10] R. Chabiniok, V.Y. Wang, M. Hadjicharalambous, L. Asner, J. Lee, M. Sermesant, E. Kuhl, A.A. Young, P. Moireau, M.P. Nash, D. Chapelle, D.A. Nordsletten, Multiphysics and multiscale modelling, data–model fusion and integration of organ physiology in the clinic: Ventricular cardiac mechanics, Interface Focus 6 (2016) 1–24.

[11] B. Cansız, K. Sveric, K. Ibrahim, R.H. Strasser, A. Linke, M. Kaliske, Towards predictive computer simulations in cardiology: Finite element analysis of personalized heart models, ZAMM Z. Angew. Math. Mech. 98 (2018) 2155–2176.

[12] K. Miller, G. Joldes, D. Lance, A. Wittek, Total Lagrangian explicit dynamics finite element algorithm for computing soft tissue deformation, Commun. Numer. Methods. Eng. 23 (2007) 121–134.

[13] F. Faure, C. Duriez, H. Delingette, J. Allard, B. Gilles, S. Marchesseau, H. Talbot, H. Courtecuisse, G. Bousquet, I. Peterlik, et al., Sofa: A multi-model framework for interactive physical simulation, in: Soft Tissue Biomechanical Modeling for Computer Assisted Surgery, Springer Berlin Heidelberg, 2012, pp. 283–321.

[14] H. Courtecuisse, J. Allard, P. Kerfriden, S.P. Bordas, S. Cotin, C. Duriez, Real-time simulation of contact and cutting of heterogeneous soft-tissues, Med. Image Anal. 18 (2014) 394–410.

[15] H. Courtecuisse, H. Jung, J. Allard, C. Duriez, D.Y. Lee, S. Cotin, GPU-based real-time soft tissue deformation with cutting and haptic feedback, Prog. Biophys. Mol. Biol. 103 (2010) 159–168.

[16] W. Hou, P.X. Liu, M. Zheng, A new model of soft tissue with constraints for interactive surgical simulation, Comput. Methods Programs Biomed. 175 (2019) 35–43.

[17] W. Hou, P.X. Liu, M. Zheng, S. Liu, A new deformation model of brain tissue for neurosurgical simulation, IEEE Trans. Instrum. Meas. 69 (2020) 1251–1258.

[18] J.A. Hernández, M.A. Caicedo, A. Ferrer, Dimensional hyper-reduction of nonlinear finite element models via empirical cubature, Comput. Methods Appl. Mech. Engrg. 313 (2017) 687–722.

[19] Z.A. Taylor, S. Crozier, S. Ourselin, A reduced order explicit dynamic finite element algorithm for surgical simulation, IEEE Trans. Med. Imaging 30 (2011) 1713–1721.

[20] A. Manzoni, D. Bonomi, A. Quarteroni, Reduced order modeling for cardiac electrophysiology and mechanics: New methodologies, challenges and perspectives, in: Mathematical and Numerical Modeling of the Cardiovascular System and Applications, Springer International Publishing, 2018, pp. 115–166.

[21] S. Deshpande, J. Lengiewicz, S.P. Bordas, Probabilistic deep learning for real-time large deformation simulations, Comput. Methods Appl. Mech. Engrg. 398 (2022) 115307.

[22] J. Song, H. Xie, Y. Zhong, J. Li, C. Gu, K.-S. Choi, Reduced-order extended kalman filter for deformable tissue simulation, J. Mech. Phys. Solids 158 (2022) 104696.

[23] H. Yang, A. Veneziani, Efficient estimation of cardiac conductivities via POD-DEIM model order reduction, Appl. Numer. Math. 115 (2017) 180–199.

[24] S. Chaturantabut, D.C. Sorensen, Nonlinear model reduction via discrete empirical interpolation, SIAM J. Sci. Comput. 32 (2010) 2737–2764.

[25] D. Bonomi, A. Manzoni, A. Quarteroni, A matrix DEIM technique for model reduction of nonlinear parametrized problems in cardiac mechanics, Comput. Methods Appl. Mech. Engrg. 324 (2017) 300–326.

[26] D. Sipp, M. Pando, P.J. Schmid, Nonlinear model reduction: a comparison between POD-Galerkin and POD-DEIM methods, Comput. & Fluids 208 (2020) 104628.

[27] S. Pagani, A. Manzoni, A. Quarteroni, Numerical approximation of parametrized problems in cardiac electrophysiology by a local reduced basis method, Comput. Methods Appl. Mech. Engrg. 340 (2018) 530–558.

[28] F. Faure, B. Gilles, G. Bousquet, D.K. Pai, Sparse meshless models of complex deformable solids, ACM Trans. Graph. 30 (2011) 1–10.

[29] B. Gilles, G. Bousquet, F. Faure, D.K. Pai, Frame-based elastic models, ACM Trans. Graph. 30 (2011) 1–12.

[30] C. Brandt, E. Eisemann, K. Hildebrandt, Hyper-reduced projective dynamics, ACM Trans. Graph. 37 (2018) 1–13.

[31] C. Romero, D. Casas, J. Pérez, M. Otaduy, Learning contact corrections for handle-based subspace dynamics, ACM Trans. Graph. 40 (2021) 1–12.

[32] C. Romero, D. Casas, M.M. Chiaramonte, M.A. Otaduy, Contact-centric deformation learning, ACM Trans. Graph. 41 (2022) 1–11.

[33] A. Jacobson, I. Baran, L. Kavan, J. Popović, O. Sorkine, Fast automatic skinning transformations, ACM Trans. Graph. 31 (2012) 1–10.

[34] J. Tapia, C. Romero, J. Pérez, M.A. Otaduy, Parametric skeletons with reduced soft-tissue deformations, in: Computer Graphics Forum, Vol. 40, Wiley Online Library, 2021, pp. 34–46.

[35] D. Baraff, A. Witkin, Large steps in cloth simulation, in: Proceedings of the 25th Annual Conference on Computer Graphics and Interactive Techniques, 1998, pp. 43–54.

[36] E. Sifakis, J. Barbic, FEM simulation of 3D deformable solids: a practitioner's guide to theory, discretization and model reduction, in: ACM SIGGRAPH 2012 Courses, 2012, pp. 1–50.

[37] S.S. An, T. Kim, D.L. James, Optimizing cubature for efficient integration of subspace deformations, ACM Trans. Graph. 27 (2008) 1–10.

[38] F.S.S. Jernej Barbič, D. Schroeder, Vega FEM library, 2012, http://www.jernejbarbic.com/vega.

[39] F.S. Sin, D. Schroeder, J. Barbič, Vega: Non-linear FEM deformable object simulator, Comput. Graph. Forum 32 (1) (2013) 36–48.

[40] J.D. Bayer, R.C. Blake, G. Plank, N.A. Trayanova, A novel rule-based algorithm for assigning myocardial fiber orientation to computational heart models, Ann. Biomed. Eng. 40 (2012) 2243–2254.

[41] O. Bernard, A. Lalande, C. Zotti, F. Cervenansky, X. Yang, P.A. Heng, I. Cetin, K. Lekadir, O. Camara, M. Ballester, Deep learning techniques for automatic MRI cardiac multi-structures segmentation and diagnosis: Is the problem solved? IEEE Trans. Med. Imaging 37 (2018) 2514–2525.

[42] D. Tang, C. Yang, T. Geva, G. Gaudette, P.J. del Nido, Multi-physics MRI-based two-layer fluid–structure interaction anisotropic models of human right and left ventricles with different patch materials: Cardiac function assessment and mechanical stress analysis, Comput. Struct. 89 (2011) 1059–1068.

[43] A.G. Gheorghe, A. Fuchs, C. Jacobsen, K.F. Kofoed, R. Møgelvang, N. Lynnerup, J. Banner, Cardiac left ventricular myocardial tissue density, evaluated by computed tomography and autopsy, BMC Med. Imaging 19 (2019) 1–9.

[44] L. Barbarotta, S. Rossi, L. Dedè, A. Quarteroni, A transmurally heterogeneous orthotropic activation model for ventricular contraction and its numerical validation, Int. J. Numer. Methods Biomed. Eng. 34 (2018) 1–24.

[45] M. Komaritzan, M. Botsch, Projective skinning, Proc. ACM Comput. Graph. Interact. Tech. 1 (2018) 1–19.

[46] L. Fulton, V. Modi, D. Duvenaud, D.I. Levin, A. Jacobson, Latent-space dynamics for reduced deformable simulation, in: Computer Graphics Forum, Vol. 38, Wiley Online Library, 2019, pp. 379–391.

[47] F. Hahn, S. Martin, B. Thomaszewski, R. Sumner, S. Coros, M. Gross, Rig-space physics, ACM Trans. Graph. 31 (2012) 1–8.

[48] J.R. Nieto, A. Susín, Cage based deformations: a survey, in: M. González Hidalgo, A. Mir Torres, J. Varona Gómez (Eds.), Deformation Models: Tracking, Animation and Applications, 2013, pp. 75–99.

[49] J.E. Zhang, S. Bang, D.I.W. Levin, A. Jacobson, Complementary dynamics, ACM Trans. Graph. 39 (6) (2020) 1–11.

[50] M.J. Moulton, B.D. Hong, T.W. Secomb, Simulation of left ventricular dynamics using a low-order mathematical model, Cardiovasc. Eng. Technol. 8 (2017) 480–494.
[51] B.D. Hong, M.J. Moulton, T.W. Secomb, Modeling left ventricular dynamics with characteristic deformation modes, Biomech. Model. Mechanobiol. 18 (2019) 1683–1696.
[52] J. Cai, F. Lin, H.S. Seah, Graphical Simulation of Deformable Models, Springer, 2016.
[53] J. Zhang, Y. Zhong, C. Gu, Deformable models for surgical simulation: a survey, IEEE Rev. Biomed. Eng. 11 (2017) 143–164.
[54] M. Hauth, O. Etzmuß, W. Straßer, Analysis of numerical methods for the simulation of deformable models, Vis. Comput. 19 (2003) 581–600.
[55] J. Allard, S. Cotin, F. Faure, P.-J. Bensoussan, F. Poyer, C. Duriez, H. Delingette, L. Grisoni, Sofa-an open source framework for medical simulation, in: MMVR 15-Medicine Meets Virtual Reality, Vol. 125, IOP Press, 2007, pp. 13–18.
[56] H.P. Bui, S. Tomar, H. Courtecuisse, S. Cotin, S.P. Bordas, Real-time error control for surgical simulation, IEEE Trans. Biomed. Eng. 65 (2017) 596–607.
[57] C.T. Kelley, Iterative Methods for Linear and Nonlinear Equations, Society for Industrial and Applied Mathematics, 1995.
[58] S.F. Johnsen, Z.A. Taylor, M.J. Clarkson, J. Hipwell, M. Modat, B. Eiben, L. Han, Y. Hu, T. Mertzanidou, D.J. Hawkes, et al., NiftySim: A GPU-based nonlinear finite element package for simulation of soft tissue biomechanics, Int. J. Comput. Assist. Radiol. Surg. 10 (2015) 1077–1095.
[59] G.A. Holzapfel, Computational biomechanics of soft biological tissue, in: Encyclopedia of Computational Mechanics, John Wiley & Sons, Ltd, 2004, chapter 18.
[60] R. de Rooij, E. Kuhl, Constitutive modeling of brain tissue: current perspectives, Appl. Mech. Rev. 68 (2016) 010801.
[61] T.J. Hughes, The Finite Element Method: Linear Static and Dynamic Finite Element Analysis, Courier Corporation, 2012.
[62] J. Tan, G. Turk, C.K. Liu, Soft body locomotion, ACM Trans. Graph. 31 (2012) 26:1–11.
[63] I. Babuška, M. Suri, Locking effects in the finite element approximation of elasticity problems, Numer. Math. 62 (1992) 439–463.
[64] M. Frâncu, A. Asgeirsson, K. Erleben, M.J. Rønnow, Locking-proof tetrahedra, ACM Trans. Graph. 40 (2) (2021) 1–17.
[65] G. Irving, C. Schroeder, R. Fedkiw, Volume conserving finite element simulations of deformable models, ACM Trans. Graph. 26 (2007) 13–es.
[66] G.R. Joldes, A. Wittek, K. Miller, Non-locking tetrahedral finite element for surgical simulation, Commun. Numer. Methods. Eng. 25 (2009) 827–836.
[67] E. De Aguiar, C. Theobalt, S. Thrun, H.-P. Seidel, Automatic conversion of mesh animations into skeleton-based animations, in: Computer Graphics Forum, Vol. 27, Wiley Online Library, 2008, pp. 389–397.
[68] G. Chen, W. Wan, K. Han, X. Feng, An automatic skinning method for real-time deformation, in: 2016 International Conference on Audio, Language and Image Processing, ICALIP, IEEE, 2016, pp. 161–165.
[69] G.R. Joldes, A. Wittek, K. Miller, Suite of finite element algorithms for accurate computation of soft tissue deformation for surgical simulation, Med. Image Anal. 13 (6) (2009) 912–919.
[70] Z. Lei, E. Rougier, E.E. Knight, L. Frash, J.W. Carey, H. Viswanathan, A non-locking composite tetrahedron element for the combined finite discrete element method, Eng. Comput. (2016).
[71] Z.A. Taylor, S. Crozier, S. Ourselin, Real-time surgical simulation using reduced order finite element analysis, in: International Conference on Medical Image Computing and Computer-Assisted Intervention, Springer, 2010, pp. 388–395.

Wenguo Hou received the B.S., M.S. and Ph.D. degrees from Beijing Jiaotong University, Beijing, China, in 2013, 2016 and 2020, respectively. He is currently a Postdoctoral Fellow with Shenzhen Institute of Advanced Technology, Chinese Academy of Sciences, Shenzhen, China.

His current research interest include modeling of soft tissue and simulation of soft robot.

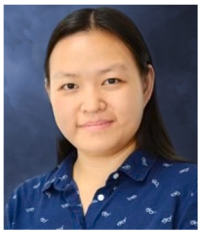

Jing Xiong received the B.S. and Ph.D. degrees from Tsinghua University, Beijing, China, in 2004 and 2010, respectively, both in mechanical engineering. She is currently a Full Professor with Shenzhen Institute of Advanced Technology, Chinese Academy of Sciences, Shenzhen, China, where she is the vice director of Research Center for Medical Robotics and Minimally Invasive Surgical Devices. She was the PI of over ten research grants, including two National Natural Science Funds, and is the founder of two industrial joint labs. She has authored or coauthored more than 60 peer-reviewed papers, and applied for over 70 patents. Her research interests include medical robotics, intelligent robotics, and image-guided therapy.

Dr. Xiong was recipient of the Wu Wenjun Artificial Intelligence Science and Technology Award (Natural Science) in 2017. She was the Program Co-Chair of IEEE RCAR 2019, and the Organizing Co-Chair of IEEE CYBER 2020.

Zeyang Xia received the B.S. degree in mechanical engineering from Shanghai Jiao Tong University, Shanghai, China, in 2002, and the Ph.D. degree in mechanical engineering from Tsinghua University, Beijing, China, in 2008. He is currently a tenured Full Professor with Shenzhen Institute of Advanced Technology, Chinese Academy of Sciences, Shenzhen, China, where he is the founding Director of the Soft Robotics Research Center. He was the PI of over twenty research grants, including the National Key Research and Development Project and four National Natural Science Funds. He has published two monographs and authored or co-authored more than 100 peer-reviewed papers, and applied for over 80 patents. His research interest focuses on robotics and biomechanics, specifically medical robotics, soft robotics, humanoid robotics, and biomechanics.

Dr. Xia was a Recipient of the Guangdong Natural Science Funds for Distinguished Young Scholar in 2015, the Wu Wenjun Artificial Intelligence Science and Technology Award (Natural Science) in 2017, and Xiong Youlun Excellent Young Scholars Award in 2019, respectively. He is the Technical Editor of IEEE/ASME Transactions on Mechatronics. He was the General Chair of IEEE RCAR 2019 and key organizing members of several other IEEE research conferences. He is the Senior Member of IEEE/CIE/CCF and has been a Fellow of IET since 2019.